Available online at www.sciencedirect.com

ScienceDirect

Transportation Research Procedia 00 (2018) 000–000

Transportation Research Procedia

www.elsevier.com/locate/procedia

International Symposium of Transport Simulation (ISTS'18) and the International Workshop on Traffic Data Collection and its Standardization (IWTDCS'18)

Traffic state estimation using small imaging satellites and connected vehicles

Toru Seo [a,b,*], Takahiko Kusakabe [c]

[a] University of Michigan, 1233 G.G. Brown, 2350 Hayward, Ann Arbor, MI 48109, The United States
[b] Tokyo Institute of Technology, 2-12-1-M1-20, O-okayama, Meguro, Tokyo 152-8552, Japan
[c] Center for Spatial Information Science, the University of Tokyo, 5-1-5 Kashiwanoha, Kashiwa-shi, Chiba 277-8568, Japan

Abstract

Small imaging satellites (SISs), which has attracted attention in remote sensing field recently, would provide a novel type of data for traffic state estimation (TSE): that is, spatial distribution of every cars in anywhere on our planet with relatively short time interval. This nature is particularly useful to complement connected vehicle (CV) data, which is sampled but time-continuous data. This paper proposes an ensemble Kalman filter-based TSE method using SIS and CV data. The proposed method endogenously estimates the fundamental diagram of traffic flow and penetration rate of CVs based only on SIS and CV data, making the method completely free from roadside detectors. The accuracy of the proposed method is verified by numerical simulation.

Keywords: remote sensing; mobile sensing; traffic flow; small satellite; connected vehicle; data assimilation

1. Introduction

Traffic state estimation (TSE), which estimates vehicular traffic state in unobserved area based on partially collected data, is essential to road traffic management. Up to the present, various types of data have been utilized for TSE purpose, such as loop detectors, global navigation satellite system-equipped *connected vehicles (CVs)*, and connected and automated vehicles (CAVs) (Seo et al., 2017a). However, each of these data types has limitations. For example, detectors do not cover wide spatial area due to sensor installation cost. CV data do not provide quantity related information, namely, flow and density; because CVs are only part of the vehicles in road network. CAVs are not widely available at this moment as they are still developing technology.

Recently, small satellites, especially *small imaging satellites (SISs)*, has attracted attention in the remote sensing field (Konecny, 2004; Sandau, 2010). Their notable feature—in fact, the definition—is their substantially smaller dimension

* Corresponding author
E-mail address: t.seo@plan.cv.titech.ac.jp

(e.g., volume less than 1 m^3 and mass less than 500 kg) compared with conventional satellites. This feature allows us to launch SISs with extremely low-cost and operate large number of them simultaneously. For example, among civilian Earth observation satellites in low Earth orbit launched during 2013–2017, approximately 350 were SISs, whereas approximately 40 were conventional satellites (based on the database provided by USC (2017)). Furthermore, the number of SIS launches is predicted to increase rapidly in the near future. This overwhelming quantity will enable us frequent, flexible, and low-cost remote sensing. For instance, a commercial SIS can capture a photo of 24 km^2 region with resolution of less than 1 m (Hayakawa et al., 2014), and a constellation consists of dozens of low Earth orbit SISs can capture photos of a specific region with less than few hours time interval (Sandau, 2010). Therefore, SISs would able to detect position of all the vehicles and therefore space-continuous density by image recognition with short time interval. Meanwhile, a major limitation of SIS data is that the time interval between two consecutive observation is still not enough to measure time-continuous traffic state variables such as speed and flow.[1]

SISs would provide a novel type of data for TSE whose nature is completely different from conventional data such as detectors and CV data: namely, spatial distribution of every cars in virtually everywhere at a time moment. This feature is particularly useful to complement CV data, which is sampled but time-continuous. On the other hand, CV data's time-continuity could be useful to complement SIS data, which has relatively long observation time interval.

The aims of this study are to formulate a TSE method that exploits SIS data and to understand basic properties of the proposed method through simulation-based analysis. Specifically, we propose a TSE method that combines SIS data and CV data in order to complement limitation of each others while not relying on any detectors.

2. Traffic observation by SIS

2.1. Observable variables and time interval

The typical observable variable by SIS observation could be location of all the individual vehicles on the surface in a particular area at a particular time moment if the weather permits. This information can be automatically obtained by applying image recognition techniques to images taken by SISs. The traffic density can then be calculated from it.

The location of observation areas and time interval of the observation mostly depend on acceptable off-nadir angle and number of SISs in the orbit. In short, the smaller the off-nadir angle, the better the imaging quality and longer the time interval; and the larger the number of SISs, the shorter the time interval. For example, time interval of observation of a mid-latitude region with 24 SISs could be approximately 7 hours with 5 degrees off-nadir angle and 1 hours with 40 degrees (Axelspace, 2017). Some of the concepts of satellite imaging is illustrated in Fig. 1.[2]

2.2. Errors of SIS observation

We analytically investigate errors of SIS observation. The overall performances of vehicle counting and density measurement by SIS observation might be affected by three types of errors: miss-detection, double-counting, and false-positive (i.e., detecting a nonexistence vehicle).

Vehicle counting error can be derived as follows. Let N be true number of vehicles in a road section of interest, X be the length of the section, and $\hat{N}$ be number of vehicles counted by SIS in the section. As technical performance parameters of SIS, let Δx_S be the spatial width of the scan window for detecting one vehicle, p_M be probability

[1] Besides SIS data, two methods that can collect spatial distribution of cars are commonly known: conventional satellites (McCord et al., 2003; Suchandt et al., 2010) and aircraft imaging (Fuse et al., 2003; Hoogendoorn et al., 2003; Coifman et al., 2006). Compared with conventional satellites, SIS has clear advantage. Namely, SIS data can be obtained with substantially shorter time interval because of their large number. Compared with aircraft imaging, SIS has advantages and disadvantages. Airplane imaging has narrower spatial coverage, but can continuously collect data for a certain time duration. Time interval of aircraft imaging might be larger than SIS, since number of such aircrafts is limited. A clear limitation of SIS and these data collection systems is that they are vulnerable to bad weather.

[2] Technical notes: The off-nadir angle is the angle from the nadir to the line of sight of a satellite. Zero off-nadir angle means that the satellite flies by the top (i.e., zenith) of the location of interest. Small off-nadir angle is especially desirable for urban traffic observation because observers need to see through concrete jungle. There is a strict relation among off-nadir angle, revisit time of a SIS, and pre-determined orbit, because SISs do not have propulsion systems. For the details on the orbital mechanics, refer, for example, Lo (1999).

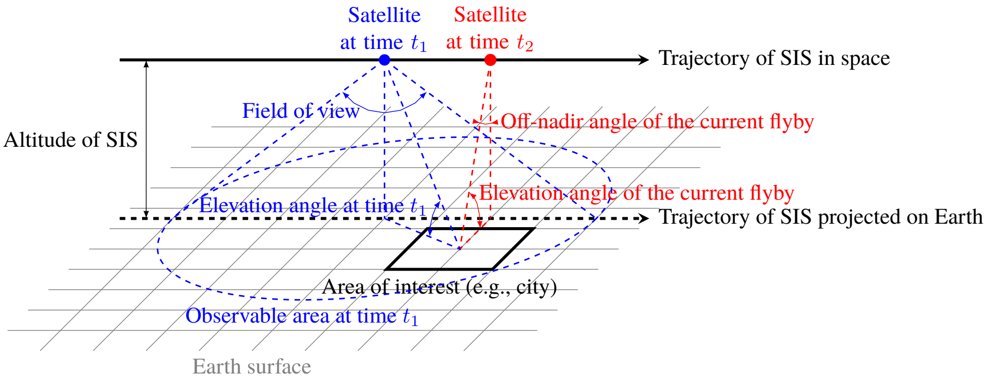

Fig. 1: Satellite flyby and its technical characteristics.

of missing a vehicle, p_D be the probability of double-counting a vehicle, and p_F be the probability of detecting a nonexistence vehicle per unit scan; these values can be given based on SIS's specification.

If there exists miss-detection error only, $\hat{N}$ follows a binomial distribution with number of trials N and success rate $1 - p_M$: namely, $\hat{N} \sim \mathcal{B}(N, 1 - p_M)$. If there exists double-counting only, $\hat{N}$ follows a shifted binomial distribution: $\hat{N} = N + \tilde{N}$ with $\tilde{N} \sim \mathcal{B}(N, p_D)$. If there exists false-positive only, $\hat{N}$ follows a shifted binomial distribution: $\hat{N} = N + \tilde{N}$ with $\tilde{N} \sim \mathcal{B}(X/\Delta x_S, p_F)$. Assuming that each of the errors is independent from the others and they can be approximated by Gaussian distributions, the entire measurement can be approximated as

$$\hat{N} \sim \mathcal{N}\left(N - p_M N + p_D N + p_F X/\Delta x_S,\ p_M(1-p_M)N + p_D(1-p_D)N + p_F(1-p_F)X/\Delta x_S\right), \tag{1}$$

where $\mathcal{N}(\mu, \sigma^2)$ represents Gaussian distribution with mean μ and variance σ^2. This can be further approximated as

$$\hat{N} \sim \mathcal{N}\left(N,\ (p_M + p_D)N + p_F X/\Delta x_S\right), \tag{2}$$

by ignoring the second order terms of p_M, p_D, and p_F, which should be substantially smaller than one, and subtracting the known bias in the mean, namely $-p_M N + p_D N + p_F X/\Delta x_S$.

Density measurement error can be derived based on the above result. Let k be true density in a road section of interest, and $\hat{k}$ be estimated density of the section by SIS. According to Eq. (2) and the definition of density (i.e., $k = N/X$), the distribution of density estimated by SIS can be approximated as

$$\hat{k} \sim \mathcal{N}\left(k,\ (p_M + p_D)k + p_F/\Delta x_S\right). \tag{3}$$

3. TSE method

3.1. Overview

We consider an estimation problem of traffic state, namely, flow, density, and speed, of traffic on a corridor. The geometry of the corridor is assumed to be known.

As traffic data collection devices, SISs and CVs are considered. The direct measurements are density measured by SIS and trajectories of CVs. Based on these measurements, following variables are inferred: *fundamental diagram (FD)*, *penetration rate (PR)* of CVs, and mean speed of traffic. Finally, the traffic density and FD are estimated by integrating (i.e., data-fusing) these information based on a data assimilation framework whose system model is a traffic flow model. In other words, distribution of the density is estimated by the data assimilation framework which takes a kind of weighted average of the model prediction (Section 3.3) and the multiple observed densities (Sections 3.4.1, 3.4.2, and 3.4.4), in which the "weight" is determined by reliabilities of these variables (i.e., procedures called "prediction" and "filtering"). Fig. 2 illustrates relation between the measurements, inferences, system model, and final estimation results.

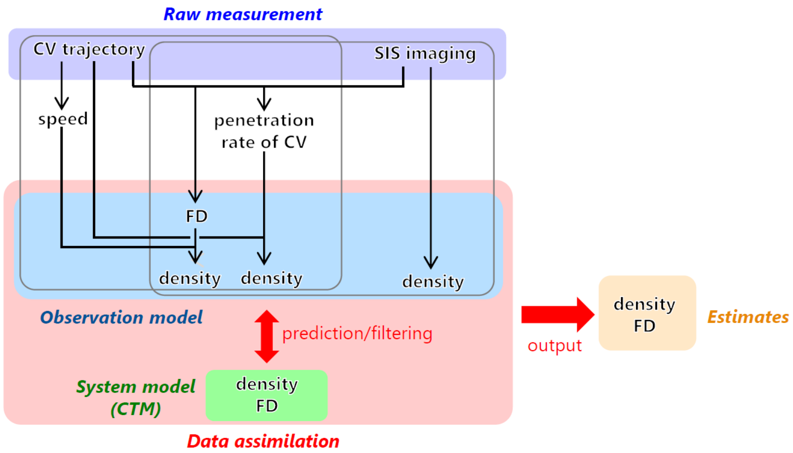

Fig. 2: Relation between the raw measurements, intermediate inferences, system model, and final estimation results.

3.2. Data assimilation

As a data assimilation framework, ensemble Kalman filter (EnKF) (Evensen, 2009) is employed. A state–space model for EnKF can be expressed as

$$\boldsymbol{x}_n = \boldsymbol{f}_n(\boldsymbol{x}_{n-1}, \boldsymbol{\nu}_n), \tag{4}$$

$$\boldsymbol{y}_n = H_n \boldsymbol{x}_n + \boldsymbol{\omega}_n, \tag{5}$$

where Eq. (4) is a system equation, Eq. (5) is an observation equation, $\boldsymbol{x}_n$ is a state vector consisting of the density and FD parameters, $\boldsymbol{f}_n$ is a system model representing a traffic flow model, $\boldsymbol{\nu}_n$ is a system noise vector, $\boldsymbol{y}_n$ is an observation vector consisting of multiple observed density and the FD parameters, H_n is an observation matrix, and $\boldsymbol{\omega}_n$ is an observation noise vector, respectively, at time step n. The observation noise vector $\boldsymbol{\omega}_n$ follows Gaussian distribution: $\boldsymbol{\omega}_n \sim \mathcal{N}(0, R_n)$.

The EnKF estimates the most probable $\boldsymbol{x}_n$ based on given $\boldsymbol{y}_n$, $\boldsymbol{f}_n$, H_n, $\boldsymbol{\nu}_n$, and R_n. For the solution procedure, see, for example, Section II.B of Seo et al. (2015). In what follows, $\boldsymbol{x}_n$, $\boldsymbol{y}_n$, $\boldsymbol{f}_n$, H_n, $\boldsymbol{\nu}_n$, and R_n are formulated to describe our TSE problem with SIS and CV.

3.3. System model

The cell transmission model (CTM) (Daganzo, 1994) is employed as the system model. The state vector $\boldsymbol{x}_n$ consists of density k_j^n, number of CVs r_j^n, respectively, in cell j at time n, and the FD parameters free-flow speed u, critical density k_c, and jam density κ, which may depend on location. The CTM can be expressed as

$$k_j^{n+1} = k_j^n + \frac{\Delta t}{\Delta x}(y(k_{j-1}^n, k_j^n) - y(k_j^n, k_{j+1}^n)), \tag{6}$$

$$y(k_{j-1}^n, k_j^n) = \min\{u k_{j-1}^n,\ q_{\max},\ (\kappa - k_j^n) u k_c/(\kappa - k_c)\}, \tag{7}$$

where Δt and Δx are time and space, respectively, discretization widths satisfying $\Delta x \geq u\Delta t$, and $q_{\max}$ is the flow capacity, which is equal to uk_c except for a bottleneck. Notice that Eqs. (6) and (7) can be rewritten in a form of $\boldsymbol{x}_{n+1} = \boldsymbol{f}_n(\boldsymbol{x}_n)$; therefore, $\boldsymbol{f}_n$ is constructed based on Eqs. (6) and (7).

The upstream boundary condition is assumed as completely unknown, as we do not have any detectors. This is represented by assuming that the density of the upstream-end cell follows uniform distributions in $[0, k_c]$. This corresponds to $\boldsymbol{\nu}_n$. The exact number of CVs r_j^n are assumed to be known, as CVs positioning is sufficiently accurate. The variable r_j^n is computed based on the cumulative count to simulate CVs traveling with the rest of traffic.

3.4. Observation model

The observation model consists of several components. Some of them infer density based on different data sources and mechanisms. The observation model aims to obtain a reliable density observation by combining these components.

3.4.1. Density measured by SIS

The density in an arbitrarily area can be directly measured when SIS observation is conducted. Let S be the set of time steps where SIS observed the traffic state. According to Eq. (3), this measurement can be approximated as

$$\hat{k}_j^n \sim \mathcal{N}(k_j^n,\ (p_M + p_D)k_j^n + p_F/\Delta x_s), \qquad \forall n \in S. \tag{8}$$

3.4.2. Density inferred by PR of CV measured by SIS

The PR of CVs in an arbitrarily area can be directly measured when SIS observation is conducted. It is reasonable to assume that the PR is a static variable; more specifically, the expected PR of unobserved period can be assumed to be identical to a recently measured PR. This information can be utilized to infer expected density of cells with CVs.

Let p_j^n be the PR of CV in cell j at time n. By the definition of the PR, the PR can be estimated by

$$\hat{p}_j^n = \frac{\sum_{i \in I_j} \sum_{m \in M_n} r_i^m}{\sum_{i \in I_j} \sum_{m \in M_n} \Delta x k_i^m}, \tag{9}$$

where I_j and M_n represent given sets of time and space where SIS observation was conducted, by which PR of (j, n) is estimated. These sets are defined as $I_j = \{i \mid j - X_I/\Delta x \leq i \leq j + X_I/\Delta x\}$ and $M_n = \{m \mid n - T_M/\Delta t \leq m \leq n,\ m \in S\}$ with given window sizes X_I and T_M, meaning that the PR is estimated using data from nearby location by recent SIS observation. Note that the number of CVs r_j^n is always known without error.

Supposing that r_j^n CVs are randomly sampled with PR p_j^n in a cell, the number of total vehicles $\Delta x k_j^n$ in the cell follows a negative binomial distribution with number of trials r_j^n and success rate $1 - p_j^n$. Therefore, by introducing Gaussian approximation, the density measured by CVs' PR can be approximated as

$$\hat{k}_j^n \sim \mathcal{N}\left(\frac{r_j^n}{\Delta x \hat{p}_j^n},\ \frac{r_j^n(1-\hat{p}_j^n)}{(\Delta x \hat{p}_j^n)^2}\right) \simeq \mathcal{N}\left(k_j^n,\ \frac{r_j^n(1-\hat{p}_j^n)}{(\Delta x \hat{p}_j^n)^2}\right). \tag{10}$$

This Gaussian approximation is accurate if p_j^n and/or $\Delta x k_j^n$ were sufficiently large.

3.4.3. FD estimated by CV and SIS

The FD parameters in a sufficiently large time–space region can be estimated by applying the methods of Seo et al. (2017b, 2018) whose inputs are trajectories of CVs and the jam density obtained by SIS. The jam density can be obtained by SISs by measuring density of cells with zero CV speed. The errors can be approximated as

$$\hat{u} \sim \mathcal{N}\left(u,\ \sigma_U^2\right), \tag{11a}$$

$$\hat{\kappa} \sim \mathcal{N}\left(\kappa,\ (p_M + p_D)\kappa + p_F/\Delta x_s\right), \tag{11b}$$

$$\hat{k}_c \sim \mathcal{N}\left(k_c,\ (p_M + p_D)k_c + p_F/\Delta x_s\right), \tag{11c}$$

based on Eq. (3), where σ_U represents an empirically known error of the FD estimation method. These estimates are directly used by the FD in the system model.

3.4.4. Density inferred by CV speed and FD

The speed in an arbitrarily time–space region can be directly measured by CVs. This can be converted to density via an FD-based mapping, although this mapping has relatively large error (Herrera and Bayen, 2010; Seo and Bayen, 2017). It can be expressed as $\hat{k}_j^n = V^{-1}(\hat{v}_j^n)$, where V represents speed–density FD (estimated by Section 3.4.3), and

v_j^n represents speed of cell j at time step n measured by CV. Thus, this mapping can be approximated as

$$\hat{k}_j^n \sim \mathcal{N}\left(k_j^n, \left(\sigma_{FD} + \frac{\sigma_V}{\sqrt{r_j^n}}\right)^2\right), \tag{12}$$

where σ_{FD} represents an empirically known error of this FD-based mapping from speed to density, $\sigma_V/\sqrt{r_j^n}$ represents speed estimation error by r_j^n CVs (Seo and Bayen, 2017), and σ_V represents its empirically known error.

3.4.5. Integration of the every observation

By integrating observation components in Sections 3.4.1–3.4.4, the observation model H_n and error R_n can be formulated. The outline of the derivation is as follows (the details are omitted due to the space limitation). Notice that the set of Eqs. (8) and (10)–(12) can be rewritten in a form of $\boldsymbol{y}_n = H_n \boldsymbol{x}_n + \boldsymbol{\omega}_n$, identical to the observation equation (5). From this fact, H_n and R_n can be formulated. Namely, H_n is a rectangular matrix that is constructed by horizontally stacking diagonal matrices whose elements are either 0 or 1 depending on the availability of each observation. The matrix R_n is a diagonal matrix whose elements corresponds to the variances in Eqs. (8) and (10)–(12).[3]

4. Verification

Quantitative features of the proposed method were verified based on numerical simulation. Specifically, relation between TSE accuracy and data quality/quantity were investigated by conducting so-called twin experiments.

4.1. Simulation setting

Traffic for 4 hours on approximately 10 km length highway with a bottleneck is considered. The FD parameters are $u = 80$ (km/h), $k_c = 30$ (veh/km), and $\kappa = 200$ (veh/km). The bottleneck is expressed by $q_{\max} = 0.6uk_c$. The discretization widths are $\Delta t = 1/120$ (h) and $\Delta x = 1.1u\Delta t \simeq 0.733$ (km). Ground truth traffic state was generated by CTM with an an appropriate initial and boundary conditions to mimic partially congested highway traffic in morning peak hours as shown in Fig. 3a; propagation and dissipation of traffic jam due to the bottleneck can be observed.

SIS observation is assumed to be conducted with a given, constant time interval Δt_S. This interval and the accuracy parameters, namely p_M, p_D, and p_F, are subjects of sensitivity analysis. The scan window for detecting one vehicle is assumed as $\Delta x_S = 0.001$ (km). Widths for PR estimation X_I, T_M are specified to cover the entire time–space region. CVs are randomly generated in the upstream boundary flow following a binomial distribution whose mean is a given PR, denoted by p_{CV}, and they travel with the rest of traffic. It means that actual PR in each cell does not necessarily identical to p_{CV}. The value of p_{CV} is also a subject of sensitivity analysis. The uncertainty of the components of the TSE method are specified as $\sigma_{FD} = 20$, $\sigma_V = 20$ (veh/km) and $\sigma_U = 5$ (km/h).

4.2. Results

The result of a base case scenario is shown in Fig. 3b as a time–space diagram. The parameters for this scenario are: $\Delta t_S = 1$ (h), $p_M = p_D = 5\%$, $p_F = 0.5\%$ (meaning that expected false-positive per km is 5 veh), and $p_{CV} = 10\%$. The estimates reproduced the ground truth fairly accurately. Its error statistics are 6.186 veh/km of root mean square error and 17.3% of mean absolute percentage error (MAPE), which can be considered as accurate TSE.

The density observed by each observation component is shown in Fig. 4. The stripe pattern in Fig. 4b means that the density estimated by PR is erroneous, because local PR is not necessarily equal to the expected PR p_{CV}. The random pattern in Fig. 4c means that the density estimated by the FD-based mapping has certain errors which is different from Fig. 4b. By comparing Fig. 4 with Fig. 3, we can confirm that the EnKF successfully estimated more accurate density by combining these relatively inaccurate observations.

[3]Note that the diagonal R_n means that correlation between observations is ignored. In reality, there may exist dependency between the observations, as easily expected by Fig. 2. However, the results in Section 4 showed that this independent observation assumption was acceptable.

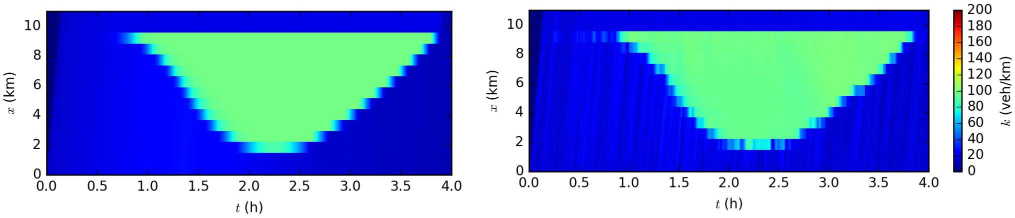

(a) Ground truth

(b) Estimate

Fig. 3: Time–space diagrams of density

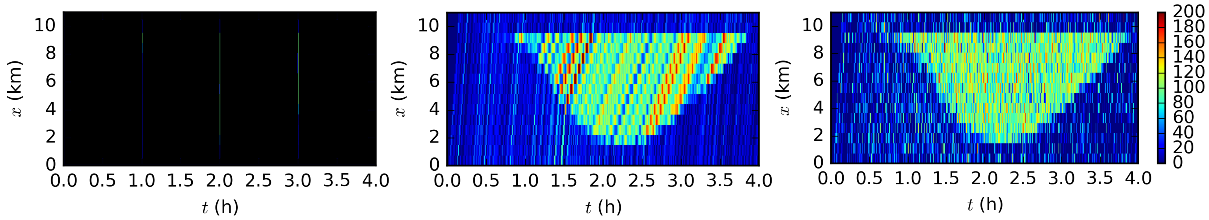

(a) SIS measurement

(b) PR-based inference

(c) Speed-based inference

Fig. 4: Each of density observations

The results of sensitivity analyses on SIS/CV data availability and SIS accuracy are shown in Fig. 5. The parameter sets are as follows: $\Delta t_S \in \{0.5, 1, 3\}$ (h), $p_{CV} \in \{1\%, 5\%, 10\%, 20\%, 50\%\}$, and $(p_M, p_D, p_F) \in \{(1\%, 1\%, 0.1\%), (5\%, 5\%, 0.5\%), (20\%, 20\%, 2\%), (50\%, 50\%, 5\%)\}$. Figure 5a shows relation between the data availability and the TSE accuracy, under a fixed accuracy. According to the figure, the TSE accuracy significantly depends on the PR of CVs; and it slightly depends on the SIS observation interval. This is a reasonable results, as the main contribution of SIS is observation of the PR and the FD but not real-time density measurement.

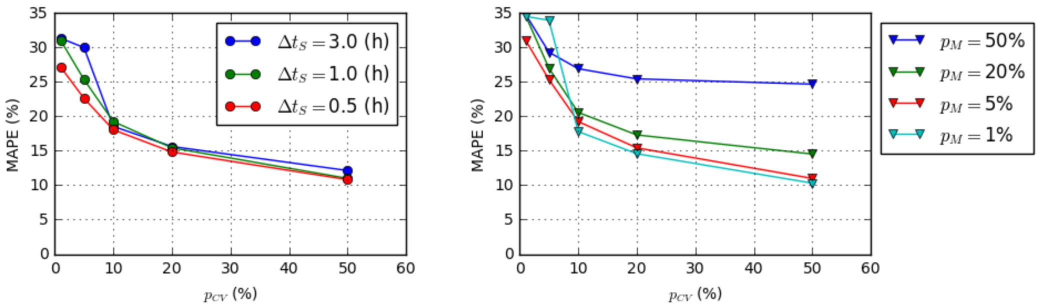

(a) $p_M = 5\%$

(b) $\Delta t_S = 1$ (h)

Fig. 5: Sensitivity analysis

Figure 5b shows relation between the SIS accuracy and the TSE accuracy. According to the figure, the TSE accuracy basically improves as the SIS accuracy improved. However, opposing to the basic tendency, the TSE accuracy is low in the cases with very small PR ($p_{CV} = 1\%, 5\%$) and very accurate SIS ($p_M = 1\%$). This can be explained as follows. When PR is small, Gaussian approximation of binomial distribution is biased and not accurate. Such inaccurate Gaussian approximation would not affect final results substantially if SIS observation is not very accurate. Contrarily, if SIS observation is accurate, such inaccurate approximation inflict negative effects to final results. To fix this issue, special consideration to the approximation error (e.g., by adding a heuristic error term to the SIS observation model) or use of the particle filter (i.e., to exclude the Gaussian approximation) are considerable.

5. Conclusion

This paper proposes a traffic state estimation method that uses small imaging satellites and connected vehicles. It endogenously estimates the fundamental diagram and penetration rate of CVs from SIS and CV data, so that the method does not require any detectors nor extensive parameter calibration. Thanks to these features, the proposed method would be useful to monitor surface traffic dynamics in large-scale areas. The accuracy of the proposed method was verified by numerical simulation. It was found that the method was capable of estimating high resolution traffic state based on accurate SIS observation combined with CVs with 10% or more penetration rate, and the independent observation assumption and the Gaussian approximation in the method were acceptable expect for extreme cases.

As an expansion of the proposed method, consideration of network traffic flow dynamics (Kawasaki et al., 2017) is valuable. Traffic volume estimation methods at signalized intersection using CV data and the FD (Wada et al., 2015; Zheng and Liu, 2017) can also be incorporated. In principle, instead of SIS, other data collection technologies such as unmanned aerial vehicles can be used without altering the formulation of the proposed TSE method; their adoption would be also interesting. Application to actual data is another important direction, as this study found that availability of SISs and CVs would be sufficient to implement the proposed method in the near future.

References

Axelspace, 2017. GRUS. https://www.axelspace.com/en/solution_/grus/, accessed: 2017-10-30.

Coifman, B., McCord, M., Mishalani, R. G., Iswalt, M., Ji, Y., 2006. Roadway traffic monitoring from an unmanned aerial vehicle. Intelligent Transport Systems, IEE Proceedings 153 (1), 11–20.

Daganzo, C. F., 1994. The cell transmission model: A dynamic representation of highway traffic consistent with the hydrodynamic theory. Transportation Research Part B: Methodological 28 (4), 269–287.

Evensen, G., 2009. Data assimilation: the ensemble Kalman filter. Springer Science & Business Media.

Fuse, T., Shimizu, E., Shimizu, T., Honda, T., 2003. Sequential image analysis of vehicle maneuvers: Evaluation of vehicle position accuracy and its applications. Journal of the Eastern Asia Society for Transportation Studies 5, 1991–2002.

Hayakawa, Y., Sakawa, N., Watanabe, K., 2014. A fabrication of the micro satellite by Canon Electronics Inc. In: Proceedings of 58th Space Sciences and Technology Conference. (in Japanese).

Herrera, J. C., Bayen, A. M., 2010. Incorporation of Lagrangian measurements in freeway traffic state estimation. Transportation Research Part B: Methodological 44 (4), 460–481.

Hoogendoorn, S., Van Zuylen, H., Schreuder, M., Gorte, B., Vosselman, G., 2003. Microscopic traffic data collection by remote sensing. Transportation Research Record: Journal of the Transportation Research Board (1855), 121–128.

Kawasaki, Y., Hara, Y., Kuwahara, M., 2017. Real-time traffic state estimation on a two-dimensional network by the state-space model. In: Proceedings of the 21st International Conference of Hong Kong Society for Transportation Studies.

Konecny, G., 2004. Small satellites – a tool for earth observation? In: ISPRS Congress Istanbul 2004. pp. 580–582.

Lo, M. W., 1999. Satellite-constellation design. Computing in Science Engineering 1 (1), 58–67.

McCord, M. R., Yang, Y., Jiang, Z., Coifman, B., Goel, P. K., 2003. Estimating annual average daily traffic from satellite imagery and air photos: Empirical results. Transportation Research Record: Journal of the Transportation Research Board 1855 (1), 136–142.

Sandau, R., 2010. Status and trends of small satellite missions for earth observation. Acta Astronautica 66 (1), 1–12.

Seo, T., Bayen, A. M., 2017. Traffic state estimation method with efficient data fusion based on the Aw–Rascle–Zhang model. In: IEEE 20th International Conference on Intelligent Transportation Systems.

Seo, T., Bayen, A. M., Kusakabe, T., Asakura, Y., 2017a. Traffic state estimation on highway: A comprehensive survey. Annual Reviews in Control 43, 128–151.

Seo, T., Kawasaki, Y., Kusakabe, T., Asakura, Y., 2018. Fundamental diagram estimation by using trajectories of probe vehicles. arXiv preprint arXiv: 1804.05927.

Seo, T., Kusakabe, T., Asakura, Y., 2015. Traffic state estimation with the advanced probe vehicles using data assimilation. In: IEEE 18th International Conference on Intelligent Transportation Systems. pp. 824–830.

Seo, T., Kusakabe, T., Asakura, Y., 2017b. Calibration of fundamental diagram using trajectories of probe vehicles: Basic formulation and heuristic algorithm. Transportation Research Procedia 21, 6–17, (Selected paper from ISTS&IWTDCS, Jeju, Korea, July 7–8, 2016).

Suchandt, S., Runge, H., Breit, H., Steinbrecher, U., Kotenkov, A., Balss, U., 2010. Automatic extraction of traffic flows using TerraSAR-X along-track interferometry. IEEE Transactions on Geoscience and Remote Sensing 48 (2), 807–819.

USC, 2017. UCS Satellite Database. UCS: Union of Concerned Scientists, http://www.ucsusa.org/nuclear-weapons/space-weapons/satellite-database, accessed: 2017-11-16.

Wada, K., Ohata, T., Kobayashi, K., Kuwahara, M., 2015. Traffic measurements on signalized arterials from vehicle trajectories. Interdisciplinary Information Sciences 21 (1), 77–85.

Zheng, J., Liu, H. X., 2017. Estimating traffic volumes for signalized intersections using connected vehicle data. Transportation Research Part C: Emerging Technologies 79, 347–362.